Sensorless Self-Commissioning of Synchronous Reluctance Machine with Rotor Self-Locking Mechanism

Sensorless Self-Commissioning of Synchronous Reluctance Machine with Rotor Self-Locking Mechanism

Anantaram Varatharajan
Department of Energy
Politecnico di Torino
Torino, Italy
anantaram.varatharajan@polito.it

Paolo Pescetto
Department of Energy
Politecnico di Torino
Torino, Italy
paolo.pescetto@polito.it

Gianmario Pellegrino
Department of Energy
Politecnico di Torino
Torino, Italy
gianmario.pellegrino@polito.it

***Abstract*—The paper proposes a sensorless technique for standstill self-commissioning of synchronous reluctance machines. Previous works have demonstrated the potential of simultaneous excitation of d and q axis with hysteresis square-wave voltage injection for the exploration of current plane with insignificant rotor movement. The proposed structure retains the hysteresis control for q axis while i_d is closed loop controlled using a weak PI regulator. Akin to the parking technique, a DC current is imposed in a fixed reference frame to inhibit any rotor movement and realize the self-locking mechanism. This permits systematic inspection of the dq current plane for accurate cross-saturation modeling. In addition, a new approach for the identification of cross-saturation in d axis from the high frequency component in i_d current is developed. The experimental tests on 1.1 kW synchronous reluctance motor test bench prove the validity of proposed technique.**

***Index Terms*—self-commissioning, magnetic model identification, flux maps, synchronous reluctance machine**

I. Introduction

Synchronous Reluctance (SyR) motors are an attractive solution for several variable speed applications, mostly because of their high efficiency, robustness, manufacturing simplicity, competitive cost and torque per volume ratio. Moreover, their highly anisotropic rotor structure inherently facilitates saliency based sensorless control at low speed, particularly useful both in low cost applications or if the reliability standards impose a safety strategy in case of encoder failure.

Most of the advanced motor control strategies require proper knowledge of machine parameters for control calibration. This necessity is more stringent in case of sensorless applications [1]. Accurate methods for detecting stator resistance and compensating inverter non-linear effects can be found in [2]. For SyR motors, the most complicated parameter to be estimated is often the current-to-flux relationship, also called flux maps, which is highly non-linear due to both self-axis saturation and cross-coupling.

The standard methods for identifying the machine magnetic model [3], [4] require to test the machine in dedicated laboratory environment. Several automatic procedures without additional hardware requirement besides the drive itself, also called self-commissioning tests, were recently developed [5]–[8].

It is worth noticing that, for sensorless drives, the commissioning stage must also be performed without adopting position transducers. Moreover, many applications require to evaluate the machine parameters without moving the rotor from its initial position (standstill constrain). Both these requirements are respected in [9]–[11], which retrieves the complete flux maps of SyR motors by exciting the machine with a proper sequence of bipolar voltage pulses, resulting in robustness against parameters uncertainty.

In this work, the control dq reference frame is aligned with the initial rotor position, detected by standard saliency based algorithm; alternatively, it can be imposed with parking technique. The magnetic model of d axis without cross-saturation ($i_q = 0$) is identified with a hysteresis square-wave voltage injection, referred as test i. Similar exploration of q axis with hysteresis square-wave voltage injection at $i_d = 0$ is referred as test ii. Then, to map the cross-saturation, the dq current plane is explored in test iii, shown in the Fig. 1. A weak PI regulator in d axis imposes an average i_d while q axis is controlled with a hysteresis square-wave injection to

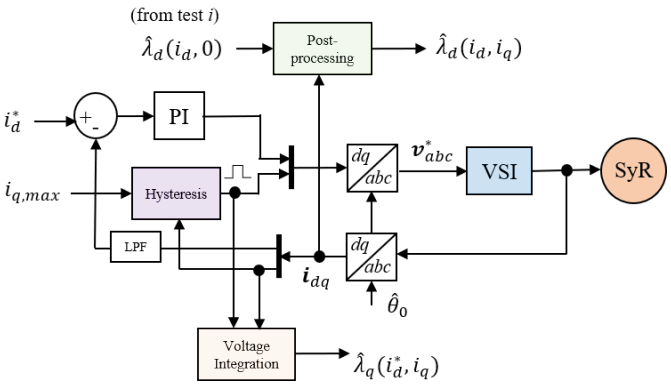

Fig. 1. Block diagram for cross-saturation identification of $\lambda_{dq}(i_d, i_q)$: test iii

ensure that the torque transients are fast enough to retain the rotor at standstill. By manipulating the PI reference i_d^* and the hysteresis limit $i_{q,max}$, the dq plane is systematically explored. The imposed DC current i_d in fixed control reference frame produces a counteracting torque if the rotor displaces from the initial position; thus, it increases stability and the permissible area of inspection. The cross-saturation phenomenon is identified from the high frequency components in i_d that are induced by the q axis hysteresis control.

The tests i and ii to identify self-saturation with hysteresis control are the same as tests #1 and #2 of [11]. To model cross-saturation effects, a test #3 is proposed in [11] where both the d and q axis are excited with hysteresis control simultaneously; it is supplemented with a sensorless position scheme to track the rotor movement. In this work, the test iii aims to replace the test #3 for a more systematic exploration of dq current plane with a self-locking to firmly hold the rotor at standstill. The major contributions of the work are:

- Increased stability and systematic inspection of dq current plane at the sensorless standstill self-commissioning conditions.
- A rotor self-locking mechanism to permit identification without a dedicated experimental rig or a mechanical locking.
- Novel technique to estimate cross-saturation from the high frequency components in a weak PI regulated i_d when the q axis is excited with a square-wave hysteresis voltage injection.

The proposed scheme is validated experimentally on a 1.1 kW, 50 Hz, 2.3 A SyR motor test bench.

II. Proposed Self-Commissioning Technique

In this work, rotor is parked to align d axis with phase a. Alternatively, the initial position can be identified by injecting an high frequency rotating voltage and capturing the minor axis of the resulting elliptical current trajectory.

Let $\hat{\theta}_0$ be the initial electrical angle of the rotor. In the succeeding text, dq denotes a fixed reference frame along $\hat{\theta}_0$. If the rotor deviates from the initial position, the error in electrical angle is given by $\tilde{\theta} = \theta - \hat{\theta}_0$. Superscript $\hat{}$ represents estimated quantities; e.g, the flux maps identified in self-commissioning are denoted by $\hat{\lambda}_d$ & $\hat{\lambda}_q$. The identification stage is composed of three tests, called test i, ii and iii.

A. Magnetic Model of SyR Machine

The stator voltage equation of a SyR machine is given by (1) where R_s is the stator resistance and ω is the electrical speed.

$$s\,\lambda_d = v_d - R_s\,i_d + \omega\,\lambda_q \tag{1a}$$

$$s\,\lambda_q = v_q - R_s\,i_q - \omega\,\lambda_d \tag{1b}$$

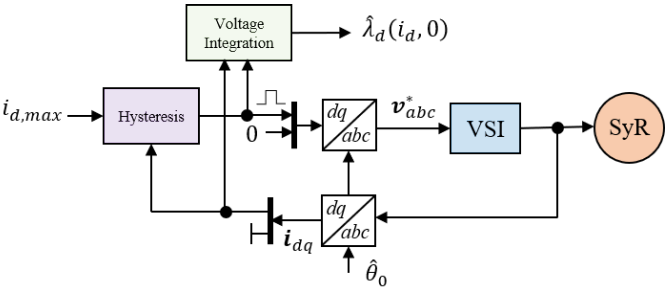

Fig. 2. Block diagram for self-saturation identification of $\lambda_d(i_d, 0)$: test i

Besides saturation along self-axis, it is known that SyR machine exhibits cross-saturation characteristics as expressed in (2).

$$\lambda_d(i_d, i_q) = \lambda_d(i_d, 0) + \int_0^{i_q} l_{dq}(i_d, \tau)\,\mathrm{d}\tau \tag{2a}$$

$$\lambda_q(i_d, i_q) = \lambda_q(0, i_q) + \int_0^{i_d} l_{dq}(\tau, i_q)\,\mathrm{d}\tau \tag{2b}$$

The incremental cross-saturation inductance l_{dq} is a function of the operating point i_d, i_q and is defined as

$$l_{dq}(i_d, i_q) = \frac{\mathrm{d}\lambda_d}{\mathrm{d}i_q} = \frac{\mathrm{d}\lambda_q}{\mathrm{d}i_d} \tag{3}$$

B. Test i & ii: identification of self-saturation

The self-saturation curves $\hat{\lambda}_d(i_d, 0)$ and $\hat{\lambda}_q(0, i_q)$ are identified through tests i and ii respectively. In test i, the d axis is excited with a square wave voltage controlled by an hysteresis mechanism, reversing the polarity of v_d whenever i_d overcomes a threshold value $i_{d,max}$. Meanwhile, v_q^* is set to zero, as shown in Fig. 2. Since the torque produced is zero, the current limit can be extended up to the machine thermal ratings without rotor movement. The flux is obtained with the voltage equation in (1) as expressed in (4a). The applied voltage is estimated from the measured DC link and the three phase duty cycles; inverter dead-time compensation is accounted for.

$$\hat{\lambda}_d(i_d, 0) = \int (\hat{v}_d - \hat{R}_s\,i_d)\mathrm{d}t \tag{4a}$$

$$\hat{\lambda}_q(0, i_q) = \int (\hat{v}_q - \hat{R}_s\,i_q)\mathrm{d}t \tag{4b}$$

In test ii, the self-saturation of q axis is identified in a similar fashion as test i where the square wave voltage pulses are applied in q axis with hysteresis limit of $i_{q,max}$ and $v_d = 0$. The flux is obtained by direct integration as in (4b). Unlike test i, hysteresis on q axis is quasi-stable and the maximum attainable $i_{q,max}$ is often determined by factors such as static friction and shaft inertia. Technique to extend the measurement area in q axis is reported in [11].

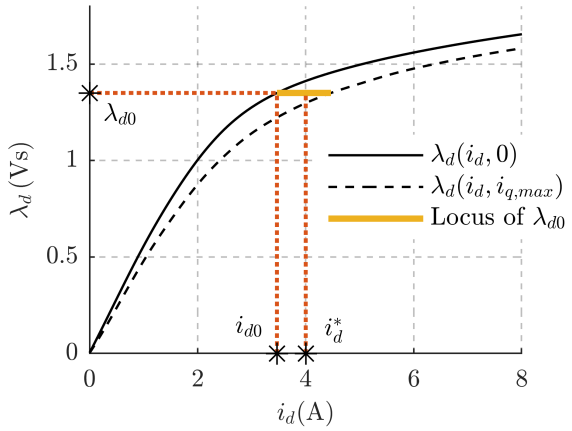

Fig. 3. Principle of the proposed cross-saturation identification in test *iii*. In yellow is the constant λ_d locus for oscillating i_d with mean i_d^*.

C. Test iii: identification of cross-saturation

To explore the dq current plane, the proposed technique exploits the propensity of rotor to align itself along the current vector (parking technique). To this end, if a sufficiently large i_d is imposed along $\hat{d}$ (fixed reference frame along $\hat{\theta}_0$), it acts as a natural locking mechanism and inhibits the rotor motion. This is realized with a PI controller on d axis and a hysteresis current control on the q axis as illustrated in Fig. 1, referred to as test *iii*. In contrast to the techniques using dual hysteresis control on d and q axis simultaneously, the proposed scheme has a larger hysteresis voltage bandwidth since the d axis consumes minimal voltage (resistive drop); consequently, faster torque reversals can be achieved. However, very high frequency leads to increase in iron losses and reduction in the acquired number of data point per cycle.

The high frequency oscillation of the q axis permeates into d axis through the cross-saturation term in (2a). If the d axis PI controller is designed such that the high frequency oscillations in i_d induced by the q axis is out of its bandwidth, then a constant flux is established as the voltage v_d^* is devoid of high frequency terms. For the reasons of symmetry, the oscillations in i_d is at twice the hysteresis frequency. It is conceptually depicted in Fig. 3 where the i_d oscillates around the mean value i_d^*, tracing the locus of a constant λ_d. This oscillation is in tandem with i_q which is hysteresis controlled with a current limit of $i_{q,max}$. The minimum value of i_d coincides with the zero-crossing of i_q, denoted by i_{d0} as depicted in the Fig. 3. The self-saturation curve (in sold line), $\lambda_d(i_d, 0)$, is available from test *i*; hence, with i_{d0} extracted from the measured current, the flux $\lambda_{d0} = \lambda_d(i_{d0}, 0)$ and subsequently, the locus of constant λ_d are determined.

III. Data Processing and Results

A. Experimental Setup

The proposed sensorless scheme is validated experimentally on a 1.1 kW SyR motor on a dspace DS1103 control platform running at a sampling frequency of 10 kHz. A picture of the setup is shown in Fig. 4. The parameters of the SyR motor under test are tabulated in Table I. The tests are performed under free shaft condition without a load to minimize shaft inertia.

Fig. 4. Experimental Setup of 1.1 kW SyR motor under test.

TABLE I
Motor Parameters

Parameters	Symbol	Values	Units
Rated Power	P_n	1.1	kW
Rated Voltage	V_n	340	V
Rated Speed	ω_n	1500	rpm
Rated Current	I_n	2.3	A
Rated Torque	T_n	7.1	Nm
Pole pairs	p	2	-
Stator Resistance	R_s	4.9	Ω
Shaft Inertia	J	0.04	kgm^2

B. Data manipulation for self-saturation (test i + test ii)

The current limit $i_{d,max}$ in test *i* is only restricted by the thermal ratings of the machine; for a short time, large currents can be acceptable. For the result shown in Fig. 5, the limits are set to $i_{d,max} = 12$A (≈3.5 p.u) and $v_d^* = \pm 220$V. A good correlation between the measured and reference curves is observed. The reference flux maps are experimentally obtained from the constant speed test [4].

As alluded to earlier, the $i_{q,max}$ in test *ii* is quasi-stable for very high current values. Hence, it is curtailed to twice the rated peak current in Fig. 5 as $i_{q,max} = 6.5$A (≈2 p.u) at $v_q^* = \pm 220$V. As with test *i*, good correlation is observed.

C. Data manipulation for $\hat{\lambda}_d(i_d, i_q)$ (test i + test iii)

For a robust self-locking mechanism in test *iii*, a minimum i_d^* is necessary; a lower limit of 0.3 p.u (1A) is recommended at free shaft. Since the machine is at standstill, a constant i_d is essentially a DC current in phase a. Hence, attention must be paid to the maximum value of i_d^* to respect thermal ratings of the machine; it is set to 2 p.u (6.5A). The step size of i_d^* is 0.1A. The hysteresis limits are set to $i_{q,max} = 6.5$A at $v_q = \pm 220$V. The PI controller is designed for a bandwidth of $\approx 2\pi \cdot 10$ rad/s; it can be calibrated with a rough estimate of inductance. To further preserve the high frequency oscillations in i_d, a low pass filter with cutoff frequency of 15 Hz is used at the feedback of PI control loop as shown in the Fig. 1.

Fig. 6 shows the test *iii* data acquired at $i_d^* = 6$A and $i_{q,max} = 6.5$A. It illustrates the high frequency components

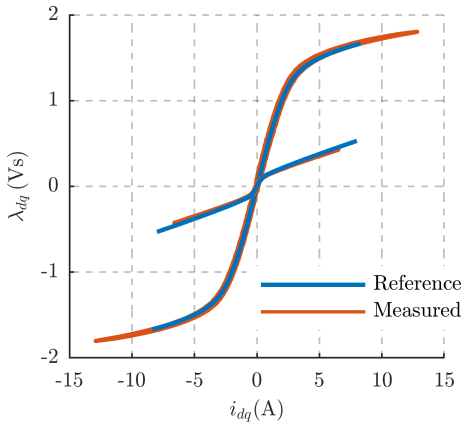

Fig. 5. Self-saturation identification of $\hat{\lambda}_d(i_d, 0)$ and $\hat{\lambda}_q(0, i_q)$ in tests i and ii respectively; shows good correlation with reference flux maps.

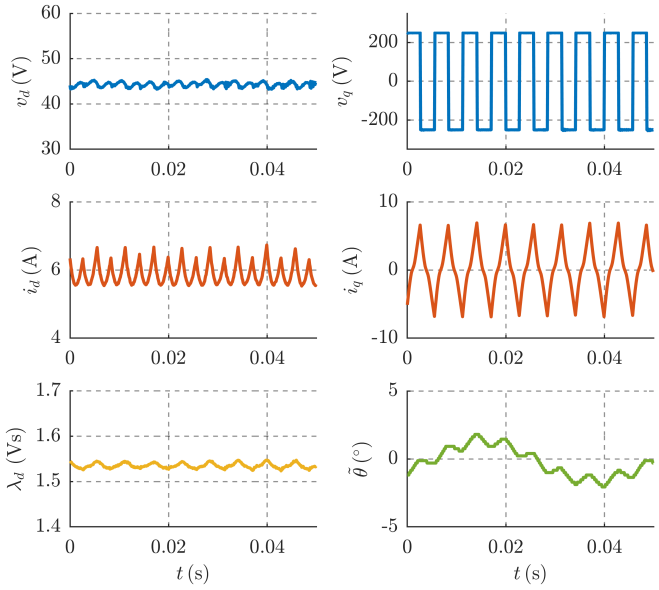

Fig. 6. Test iii data recording at $i_d^* = 6$A and $i_{q,max} = 6.5$A; illustrates high frequency oscillations in i_d, relatively constant v_d and λ_d, and confined rotor movement $|\tilde{\theta}| < 2°$.

of i_d at twice the hysteresis frequency. Moreover, it can be observed that the weak PI controller generates a relatively constant v_d and thereby, reasoning the assumption of constant λ_d. It is worth pointing out that the rotor movement is restricted to $|\tilde{\theta}| < 2°$, validating the self-locking mechanism.

Fig. 7 shows the data acquired in test iii for selected values of i_d^*. The high frequency oscillations in i_d are superimposed over the reference flux maps to draw parallels from Fig. 3 and to illustrate the relatively constant λ_d. Fig. 8 shows the corresponding current trajectories whose increasing convex nature with i_d^* is a testament to the cross-saturation phenomenon.

The results obtained for each i_d^* value were interpolated with a quadratic polynomial function (dotted lines in Fig. 8) whose equation is reported in (5), where i_{d0} is the self-saturation term depicted in Fig. 3 and a_1 and a_2 are the first and second order coefficients. The absolute value of $|i_q|$ is used due to symmetry.

$$i_d(\lambda_d, |i_q|) = i_{d0}(\lambda_d) + a_1(\lambda_d) \cdot |i_q| + a_2(\lambda_d) \cdot |i_q|^2 \quad (5)$$

This expression (5) represents locus of constant λ_d; the value of λ_d is interpolated from the results of test i using i_{d0} as $\hat{\lambda}_d(i_{d0}, 0)$. Fig. 9 represents the coefficients in (5) as a function of λ_d. Each data point in Fig. 9 represents a unique measurement set for various i_d^*. It can be observed that the data points are absent for low magnitudes of flux due to the imposed minimum i_d^* for rotor locking. In order to extrapolate, a higher order polynomial fitting is undertaken, in the nature of (6).

$$\begin{aligned} a_1(\lambda_d) &= a_{11} \cdot \lambda_d + a_{15} \cdot \lambda_d^5 \\ a_2(\lambda_d) &= a_{21} \cdot \lambda_d + a_{25} \cdot \lambda_d^5 \end{aligned} \quad (6)$$

Thus, with the integration of tests i and iii, the four coefficients in (6) are estimated and in turn, the complete map of $i_d(\lambda_d, |i_q|)$ becomes realizable. Upon simple manipulations, the direct flux map $\lambda_d(i_d, i_q)$ is obtained.

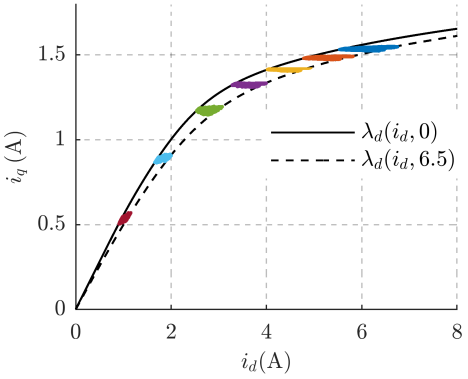

Fig. 7. Test iii for cross-saturation identification. Data acquired for different i_d^* at $i_{q,max} = 6.5$A. High frequency oscillations of i_d projected over the reference flux maps to illustrate constant λ_d.

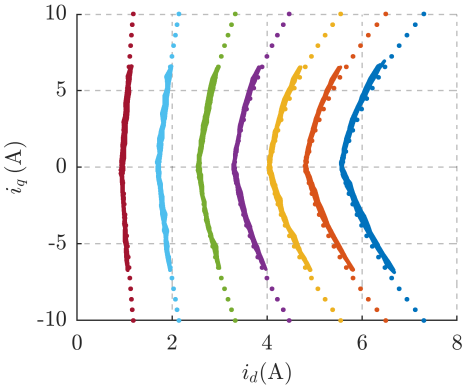

Fig. 8. Current trajectories on constant λ_d locus traced during test iii. Dotted lines denote the quadratic polynomial fitting (5). Note that identical color code to that of Fig. 7 is used for ease of comparison

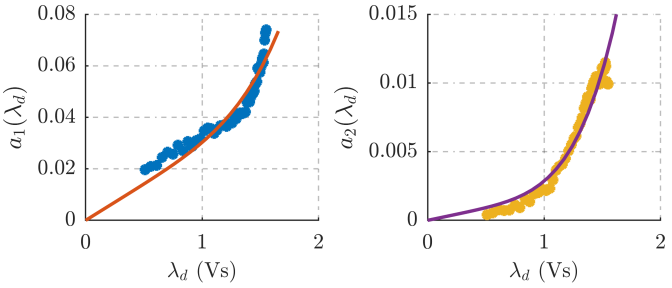

Fig. 9. Coefficients of constant λ_d locus and the best-fit polynomial (6): (a) $a_1(\lambda_d)$; (b) $a_2(\lambda_d)$

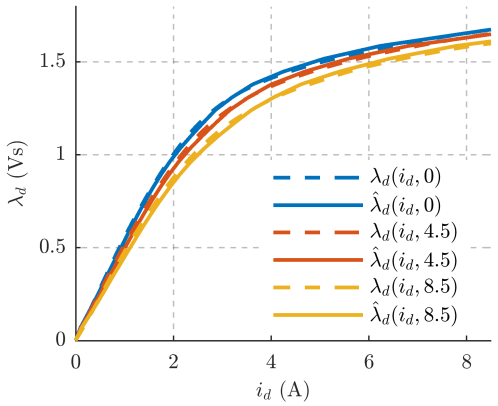

Fig. 10. Comparison of self-commissioning vs. reference flux maps for d axis.

Fig. 10 shows the identified flux curves with self-commissioning; a good correlation with reference curves is observed. Despite the limited exploration of q axis with maximum $i_{q,max} = 6.5$A, the estimated $\hat{\lambda}_d(i_d, 8.5)$ shows good correspondence with the reference, validating the extrapolation coefficients. A comprehensive comparison is reported in the Fig. 11 by computing the flux error contour in dq current plane; the error is confined to less than 3% of rated flux, predominantly in the vicinity of knee-point. The region of exploration is denoted by a black box to highlight the potential of proposed technique to extrapolate with good accuracy.

D. Data manipulation for $\hat{\lambda}_q(i_d, i_q)$ (test ii + test iii)

The data processing for q axis flux maps is largely simplified due to the application of hysteresis control. Akin to the self-saturation identification in test ii, direct integration of hysteresis voltage is also applicable for test iii as in (7). For simplicity, the i_d is approximated to the reference value, i_d^*. Thus, it is a straightforward estimation of the flux curves $\hat{\lambda}_q(i_d^*, i_q)$ for points within the region of exploration.

$$\hat{\lambda}_q(i_d^*, i_q) = \int (\hat{v}_q - R_s\, i_q)\mathrm{d}t \tag{7}$$

To compute flux beyond the explored region, the dq current plane is segmented into three regions as shown in the Fig. 12. Upon saturation, the q axis exhibits a largely constant

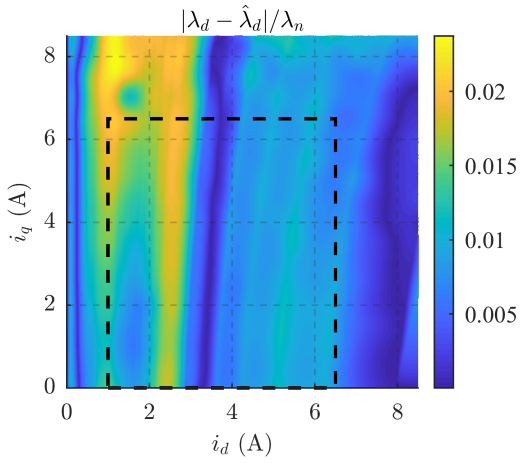

Fig. 11. Error contour of d axis flux maps in p.u. Maximum error 3% of rated flux in vicinity of knee-point is observed. Dotted black box denotes the region of exploration.

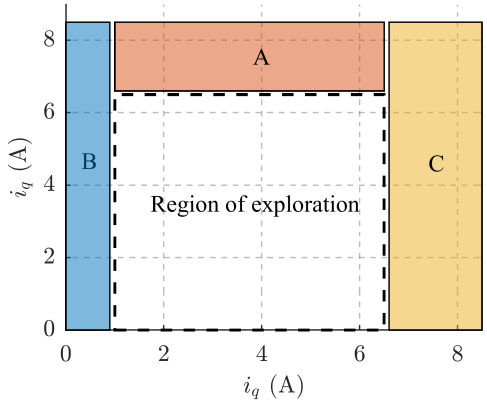

Fig. 12. Segmented regions (A,B and C) for flux estimation beyond the region of exploration.

incremental inductance; this property is exploited in region A where the flux curves are linearly extrapolated by computing the saturated inductance. Region B is bounded by the curve from test ii to the left and test iii to the right. Hence, a simple linear interpolation is sufficient.

In the case of region C, the reciprocity property (3) of cross-saturation inductance l_{dq} is exploited. For each operating point, the term $l_{dq}(i_d, i_q)$ is computed from the d axis flux maps. Then, with the boundary of explored region as the starting point, $\hat{\lambda}_q$ is estimated progressively to the right using (2b).

Fig. 13 shows the identified q axis curves with self-commissioning; a discrepancy with reference maps is seen. The absolute error is ≈5% at the rated peak current and increases at overload. This error can be attributed to iron losses that are further magnified owing to the high hysteresis frequency, in the range of 175 Hz. Fig. 14 provides the comprehensive error contour where the maximum error is $< 3\%$ of the rated flux.

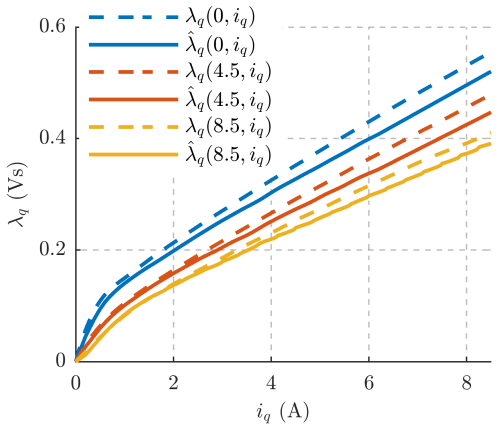

Fig. 13. Comparison of self-commissioning vs. reference flux maps for q axis.

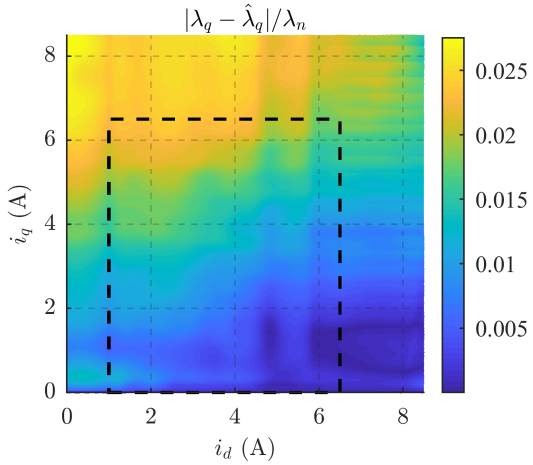

Fig. 14. Error contour of q axis flux maps in p.u. Maximum error 3% of rated flux at high overload is observed. Dotted black box denotes the region of exploration.

IV. Conclusion

The proposed technique attempts to identify the magnetic model of SyR machines under sensorless standstill self-commissioning constraints. In particular, the emphasis is placed on accurate assessment of cross-saturation effect with systematic exploration of regions of interest. To this end, a new scheme is developed by integrating PI and hysteresis controllers in d and q axis respectively, on a fixed reference frame to realize a rotor self-locking mechanism. This aids in counteracting the high frequency torque oscillations from hysteresis control and holds the rotor firmly still, as demonstrated experimentally. Furthermore, a novel technique to extract the cross-saturation effect from the induced high frequency current in d axis is developed. Experimental validation on a 1.1 kW SyR machine test bench shows good correlation with reference flux maps where the error is in order of $< 3\%$ of rated flux.

References

[1] N. Bianchi, E. Fornasiero, and S. Bolognani, "Effect of stator and rotor saturation on sensorless rotor position detection," in *IEEE Transactions on Industry Applications*, vol. 49, no. 3, 2013, pp. 1333–1342.

[2] R. Antonello, L. Ortombina, F. Tinazzi, and M. Zigliotto, "Online stator resistance tracking for reluctance and interior permanent magnet synchronous motors," in *2017 IEEE Energy Conversion Congress and Exposition (ECCE)*, 2017, pp. 5861–5868.

[3] IEEE, "IEEE Trial-Use Guide for Testing Permanent Magnet Machines," pp. 1–56, 2015.

[4] E. Armando, R. I. Bojoi, P. Guglielmi, G. Pellegrino, and M. Pastorelli, "Experimental identification of the magnetic model of synchronous machines," *IEEE Transactions on Industry Applications*, vol. 49, no. 5, pp. 2116–2125, 2013.

[5] S. M. Yang and K. W. Lin, "Automatic Control Loop Tuning for Permanent-Magnet AC Servo Motor Drives," *IEEE Transactions on Industrial Electronics*, vol. 63, no. 3, pp. 1499–1506, 2016.

[6] L. Peretti, P. Sandulescu, and G. Zanuso, "Self-commissioning of flux linkage curves of synchronous reluctance machines in quasi-standstill condition," *IET Electric Power Applications*, vol. 9, no. 9, pp. 642–651, 2015.

[7] G. Pellegrino, B. Boazzo, and T. M. Jahns, "Magnetic Model Self-Identification for PM Synchronous Machine Drives," pp. 2246–2254, 2015.

[8] S. A. Odhano, R. Bojoi, S. G. Rosu, and A. Tenconi, "Identification of the magnetic model of permanent magnet synchronous machines using DC-biased low frequency AC signal injection," in *2014 IEEE Energy Conversion Congress and Exposition (ECCE)*, 2014, pp. 1722–1728.

[9] N. Bedetti, S. Calligaro, and R. Petrella, "Stand-Still Self-Identification of Flux Characteristics for Synchronous Reluctance Machines Using Novel Saturation Approximating Function and Multiple Linear Regression," pp. 3083–3092, 2016.

[10] M. Hinkkanen, P. Pescetto, E. Mölsä, S. E. Saarakkala, G. Pellegrino, and R. Bojoi, "Sensorless Self-Commissioning of Synchronous Reluctance Motors at Standstill Without Rotor Locking," *IEEE Transactions on Industry Applications*, vol. 53, no. 3, pp. 2120–2129, 2017.

[11] P. Pescetto and G. Pellegrino, "Automatic Tuning for Sensorless Commissioning of Synchronous Reluctance Machines Augmented with High-Frequency Voltage Injection," *IEEE Transactions on Industry Applications*, vol. 54, no. 5, pp. 4485–4493, 2018.